Nonlinear Dyn (2025) 113:16301–16317
https://doi.org/10.1007/s11071-025-11019-0

RESEARCH

Nonlinear displacement control and force estimation in a piezoelectric robotic manipulator characterizing an object with nonlinear viscoelastic deformation

Gerardo Flores · Micky Rakotondrabe

Received: 21 April 2024 / Accepted: 17 February 2025 / Published online: 10 March 2025

Abstract This paper presents the modeling and control of a piezoelectric robotic manipulator designed to characterize the behavior of a deformable object exhibiting nonlinear and viscoelastic deformation. The manipulator's nonlinear dynamics are approximated using a classical Bouc-Wen hysteresis model, which captures its inherent hysteretic behavior. An output feedback control law is developed to ensure accurate position reference tracking for the manipulator. The control strategy leverages state observers to estimate both the manipulator's states and the interaction force with the deformable object. By combining the estimated interaction force with the controlled position data, the force-deformation characteristics of the object are analyzed, providing insight into its behavior and enabling the potential identification of its model parameters. The robustness of the proposed approach is demonstrated through simulations and experiments, where Gaussian noise was added to the system to evaluate its performance under realistic conditions.

Keywords Object characterization · Piezoelectric manipulator · Output feedback position control · Nonlinearities

Mathematics Subject Classification 70Q05 · 93C85 · 74N30 · 93D15

List of symbols

α_1	Actuator's dynamics parameter
$\bar{\varepsilon}_1, \bar{\varepsilon}_2$	Change of coordinates, $\bar{\varepsilon}_1 = \varepsilon_1, \bar{\varepsilon}_2 = \varepsilon_2 - g(\varepsilon_1)$
$\Delta(t)$	Unknown term equal to $-h - c_p F$
$\delta_y(t), \delta_h(t)$	Unknown terms, $\delta_y(t) = -\frac{c_p}{\alpha_1} F$; $\delta_h(t)$ is the hysteresis disturbance
$\eta_y(t), \eta_h(t),$	$\eta_u(t), \eta_m(t)$ Gaussian noise affecting the system, hysteresis, control, and measurement, respectively
$\hat{(\cdot)}$	Estimated of $(\cdot)$
$\psi[.]$	Nonlinear elastic behavior
τ_o	Viscous deformation parameter
$\varepsilon_1, \varepsilon_2$	Observer errors $\varepsilon_1 = \hat{y} - y$, $\varepsilon_2 = \hat{\Delta}(t) - \Delta(t)$
ϱ	Positive parameter for (5)
$A_{bw}, B_{bw}, \Gamma_{bw}$	Hysteresis parameters considered known
c_p	Actuator's mechanical compliance

A part of this work was presented at the American Control Conference held in Toronto, Canada, in July 2024.

G. Flores (✉)
RAPTOR Lab, School of Engineering, College of Arts and Sciences, Texas A&M International University, 5201 University Boulevard, Laredo, Texas 78041, USA
e-mail: gerardo.flores@tamiu.edu

M. Rakotondrabe
Laboratoire Génie de Production, University of Technology of Tarbes (UTTOP), University of Toulouse alliance, 47 Avenue d'Azereix, 65000 Tarbes, Hautes-Pyrénées, France
e-mail: mrakoton@uttop.fr

d_p	Piezoelectric coefficient
e	Tracking error $e = y - y_d$
F	External force applied to the actuator
F_o	Force applied by the actuator to an external object
h	Hysteresis state
k	Control gain
k_1, k_2, κ, θ	Observer gains
$S \in \mathbb{R}^{2\times 2}$	Observer gain and solution of (26)
u	Control input
y	Measured displacement
$y_d(t)$	Desired position
$z = \left(y,\ h\right)^\intercal$	Vector state

1 Introduction

Understanding the behavior of highly deformable objects such as textiles is paramount in numerous applications. For instance, the behavior properties of technical textiles can be accounted for when designing textiles composites based structures that require rigorous performances like in automotive, aeronautical, medical, defense, sports, and energy production applications [2]. According to the behavior of interest (chemical, thermal, toxicity, aging, mechanical, etc.), different methods are used for the characterization [3]. For mechanical behavior, precisely the nonlinear and viscoelastic characteristics, the tests are generally led with a tensile/contraction mechanical machine with which the deformation velocity is controlled and the tensile or the compression force is measured [4]. However, controlling the position, and thus the deformation itself, rather than the velocity while characterizing objects, opens more possibilities. Not only it is still possible to do velocity control by imposing constant slope deformation as a reference, but most importantly, position control allows us to directly observe the different objects' critical points: the elastic deformation limit, plastic deformation, and the break-point. Lastly, because the strain/stress map is the most used characteristic, controlling the deformation during characterization is more meaningful than controlling the velocity.

Because standard tensile/contraction machines are limited to velocity control, robotic systems have been recently used to perform position/deformation-controlled object characterization. The advantage of robotic systems is that switching to force control is possible. For instance, a 6-DOF KUKA K120 has been used to measure and characterize the properties of 100% flax fiber fabrics [5]. Such a robotic system can apply hundreds of Newtons of force to the object and several centimeters of deformation of the latter while exhibiting a hundred microns of accuracy. However, in some applications such as fibers-based skin attachable monitoring devices [6], the textile material characterization might require a force range of less than one Newton, force resolution better than the milliNewton, deformation ranges up to a few millimeters only and deformation resolution in the order of a micron. In this case, industrial robotics can no longer be used. Instead, piezoelectric robotic manipulators are one of the best candidates. Indeed, they can offer tens of nanometer positioning resolution, relatively large bandwidth (hundreds of Hertz), and highly resolute force, which are properties that are compatible with the above requirements [7]. In counterpart, piezoelectric actuators exhibit strong hysteresis nonlinearity, which challenges the final accuracy or even the stability of the tasks if not adequately controlled. Moreover, during the characterization tasks, the interaction force with the object also acts as a disturbance that affects the accuracy. The context of this paper is to control the position of a piezoelectric manipulator that is used to characterize a miniaturized and deformable textile object, as described in Fig. 1. A piezoelectric actuator generates a displacement y when a voltage u is applied. This displacement is amplified (or attenuated), reversed through a two-levers-based frame, and applied to the textile object's extension (deformation) y_o. The reaction force F_o of the textile is proportional to the force F

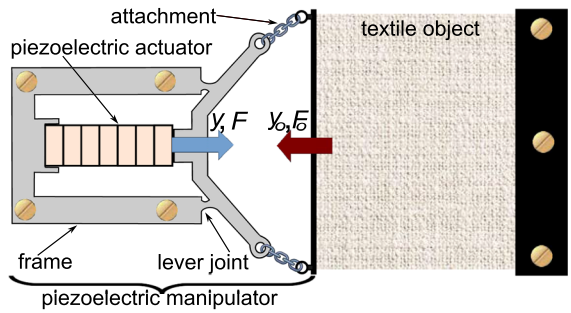

Fig. 1 Object characterization. Only tensile force can be applied with the technological tool and piezoelectric manipulator. The piezoelectric actuator (in the middle) is a piezoelectric "stack" type that can only elongate when a voltage is applied to it; the blue arrow at the actuator tip represents this elongation. Then, the lever mechanism inverts the direction of the movement, and as a consequence, the attachments (chain-like) will pull the textile object, as represented by the red arrow

that resists the actuator movement. As a consequence, a plotting of (y_o, F_o) allows to have the *(deformation, force)*-characteristics of the textile, which finally will result in its strain–stress property. The piezoelectric actuator that will be used to develop the characterization platform is a piezoelectric stack (also known as piezostack) from *PiezoDrive* company and has dimensions: width x height x length $= 7mm \times 7mm \times 42mm$. It can provide a displacement up to $70\mu m$ for a maximal voltage of $150V$.

The literature on control of piezoelectric actuators and manipulators is dense. The different works can be categorized into feedforward (or open-loop) control architecture and feedback control architecture. The principle of feedforward control architecture consists of compensating for the undesired behavior inside the piezoelectric manipulator by using a cascade controller without any feedback. This controller, also called a compensator, is a kind of inverse model of the undesired behavior. For instance, the hysteresis nonlinearity was compensated for by using the exact inverse and the approximate-inverse of the classical Preisach model in [8] and in [9] respectively, using the exact inverse and the approximate-inverse of the classical Prandtl-Ishlinskii model in [10] and in [11] respectively, using the exact inverse of the Rate-Dependent Prandtl-Ishlinskii model in [12], and using the approximate inverse of the classical Bouc-wen model in [13,14]. Additionally to the hysteresis nonlinearity, the creep and the badly damped phenomena have also been feedforward controlled simultaneously by using cascade compensators in [15–17]. Feedforward control architecture features low cost and ease of technological implementation because no external sensors are used. It is specifically suitable for micro and nanopositioning because there is a strong lack of appropriate sensors for such application. In counterpart, this architecture is known for its lack of robustness against model uncertainties and against external disturbances. Because the application in this paper deals with the interaction between a piezoelectric manipulator and an object, feedforward control architecture is not suitable due to the interaction force that acts as an external disturbance to the manipulator.

Regarding the feedback control architecture of piezoelectric manipulators and actuators, two categories can also be found: model-based and non-model-based control approaches, depending on whether or not the hysteresis model is used to synthesize the feedback controller. In the non-model-based control approach, primary works directly designed controllers by assuming that the manipulator is linear [18,19]. They are only efficient if the piezoelectric manipulators operate at low output displacement, which generates a low hysteresis phenomenon. For large output displacement operations in which the hysteresis becomes non-negligible, the non-model-based control approach consists in compensating for the hysteresis first with a feedforward controller and then designing the feedback controller by using the resulting linear model [20]. As a consequence, because the non-model-based control design does not consider the hysteresis model explicitly during the feedback controller design, there is no guarantee about the stability of the feedback against the presence of the hysteresis phenomenon and against its size.

Contrary to non-model-based, the model-based control approach permits to explicitly account for the hysteresis during the synthesis of the feedback controller, or permits to analyze the stability for a given feedback that contains hysteresis phenomenon. In [21], the authors proposed to combine the small-gain theorem with the classical Prandtl-Ishlinskii hysteresis model to find the stability condition of the feedback. However, due to the superposition of operators nature and structure of the Prandtl-Ishlinskii modeling approach, it is generally not preferred for analytical analysis and synthesis. Instead, the Bouc-Wen modeling approach is more suitable because it is based on differential equations with fewer parameters. The classical Bouc-Wen hysteresis model was used to design stabilizing sliding mode control laws in [22,23], to design adaptive sliding mocde control laws in [24–26], and backstepping control laws in [27,28]. The general principle consists of estimating the hysteresis state thanks to a converging observer (for instance, with a linear-extended-state-observer or a nonlinear observer) and then compensating for it in the feedback control. In those works, only the displacement (position) of piezoelectric manipulators was controlled, and no interaction was made with an object. Recently, in [29], an output position feedback control was proposed while the piezoelectric actuator was subjected to an interaction force with an object. However, the force was considered a disturbance to be rejected only and was not estimated. Yet, knowing the force is essential during the characterization of an object, as this information allows one to extract the object's characteristics.

1.1 Contribution

This paper proposes to displacement (position) control a piezoelectric manipulator interacting with an object while simultaneously estimating the interaction force for characterization purposes and explicitly considering the hysteresis in the controller design. The contributions are:

i) the consideration of both the actuator hysteresis and the interaction force in the controller design. The classical Bouc-Wen model is specifically used to model the actuator hysteresis while the force is an external disturbance.
ii) the design of observers, which allows us to estimate the dynamical states, the hysteresis state of the actuator, and the force.
iii) and the application to a textile object characterization. It is worth noting that the observer and the controller designs do not need any information regarding the object behavior (model, structure, parameters). Thus, the approach can be used to characterize any object without any prior knowledge of it.

1.2 Content

The remainder of the paper contains the following:

1. First, a displacement control law and force estimation are designed using only the actuator model, which contains hysteresis nonlinearity. No object model is used on it. The control law and the observer designs are in Sect. 4 and Sect. 3, respectively.
2. Then, the control law and observer are simulated when applied to the actuator model. A simulation uses a force as an external disturbance using a signal generator. The observer estimates the entire disturbance Δ (including the force disturbance) in the simulation results. This part is presented in Sect. 5.1.
3. Afterward, the control law and the observer are simulated when applied to the actuator model interconnected with an object model (the model in (51)) rather than to the actuator model alone. This is the aim of Sect. 5.3.
4. Still in Sect. 5.3, the force estimated by the observer during the simulation in step 3) is plotted versus the controlled output displacement of the actuator (which does correspond to the object's deformation as they are assumed to be initially in contact). This plot is compared with the force-displacement plot obtained only from (51). The result in Fig. 9 shows consistency, which leads us to conclude that the control law and the observer, designed without an object model, can be used to characterize the latter.
5. The paper is concluded with some final remarks in Sect. 6.

2 Problem formulation

The classical Bouc-Wen hysteresis with first-order dynamics describes the actuator behavior:

$$\Sigma : \begin{cases} \alpha_1 \frac{dy}{dt} + y = d_p u \overbrace{-h - c_p F}^{=\Delta(t)} \\ \frac{dh}{dt} = A_{bw} \frac{du}{dt} - B_{bw} \left| \frac{du}{dt} \right| h - \Gamma_{bw} \frac{du}{dt} |h| + \delta_h(t) \end{cases} \tag{1}$$

where: A_{bw}, B_{bw}, and Γ_{bw} are known constants parameters for the hysteresis subsystem, d_p is the piezoelectric coefficient, c_p is the actuator' mechanical compliance, and $\alpha_1 > 0$ is the actuator' dynamics parameter. The internal hysteresis state is represented by h. The external force applied to the actuator is equal to $F = -F_o$, in which F_o is the force applied by the actuator to any external object. We denote $\Delta(t) = -h - c_p F$.

The second equation of the model in (1) describes the hysteresis evolution in which A_{bw}, B_{bw} and Γ_{bw} define its shape and amplitude. The $\delta_h(t)$ represents unmodeled terms and exogenous signals [30]. It is worth noting that because piezoelectric actuators and manipulators generally exhibit badly damped vibrations, a periodic second-order model at least is more representative of their dynamics [31], [32]. Notwithstanding, a feedforward controller is first recommended to dampen the vibrations before synthesizing a feedback controller. The reasons are that designing a feedback control law straightaway from a badly damped system leads to a loss of bandwidth and a weakness of the stability margins. Hence, the piezoelectric manipulator considered in this paper beforehand encompasses a feedforward compensation of the badly damped vibrations, in which case a first-order model is sufficient as is the case in previous works [29], [33].

On the other hand, the textile object deformation is given by the following nonlinear viscoelastic model [34]:

$$\Omega : \left\{ \tau_o \frac{dy}{dt} + y = \psi[F] \right. \tag{2}$$

in which τ_o is the viscous deformation parameter and $\psi[.]$ represents the nonlinear elastic behavior. There are two approaches to modeling textile objects [35]: i) analytical and ii) numerical, mainly through finite element theory. The analytical approach (see (2) and (51)) was chosen to represent the object model because it is easier to simulate for the validation of the proposed characterization technique with the proposed control law and observer. In the analytical approach, among the existing models in the static regime are: i) power law [36,37], and ii) tensor-based model [38]. The former is more straightforward than the latter.

Once the system (Σ, Ω) is defined, the problem under consideration can be formally stated as follows.

Problem 1 *The system* (Σ, Ω) *is considered together with the following assumptions:*

Assumption 1 The force F, the state h, and the velocity $\frac{dy}{dt}$ are not measured.

Assumption 2 The parameters of the system Ω in (2) are entirely unknown, including τ_o, the structure of $\psi[\cdot]$, and the parameters contained within it.

Assumption 3 The parameters of the system Σ in (1) are fully known, as they can be estimated or identified using well-established techniques extensively explored in the literature [13,39].

The primary objective is to design an appropriate control law $u(\cdot)$ for the actuator to ensure stabilization while allowing the displacement (position) y to track a desired reference y_d, **relying solely on measurements of the displacement** y. Additionally, the actuator must interact with the object being characterized through the force F.

2.1 Proposed solution

To address the above problem, the proposed approach is illustrated in Fig. 2 and summarized below.

- In the first place, an estimation of the actuator's dynamics state $(y, \frac{dy}{dt})^T$ is proposed. The observer also estimates the "disturbance" $\Delta = -(h + c_p F)$.
- Then, an observer that estimates h is designed.
- Having $\hat{\Delta}$ and $\hat{h}$, an estimation of F is derived.
- Afterwards, a control law is designed based on the output y, on the estimate states, and on $\hat{h}$.
- Last, the controlled ouptut y and the estimate force $\hat{F}$ are used to plot (y_o, F_o) characteristics of the textile object, where $y_o = k_m y$ and $F_o = \frac{1}{k_m}\hat{F}$ in which k_m is the lever mechanism gain. Without loss of generality, $k_m = 1$ is taken.

Remark 1 The two main reasons for interest in using position control rather than velocity control for object characterization are:

- Besides relaxation (which involves characterization with constant deformation velocity), the primary focus of object characterization lies in understanding the deformation itself-thereby controlling its position-and the corresponding force or stress. This approach enables us to visualize the (stress, deformation) characteristics, identify key points on the resulting graph (such as the elastic limit and critical breakpoints), delineate between linear and nonlinear domains, discern various types of object behavior, and deduce essential parameters like the Young modulus (the ratio between stress and deformation).
- Controlling the velocity and using an integral to estimate the deformation is sensitive to initial value bias, while identifying the initial value for each object to be characterized is impractical.

3 Observers design

This section proposes an observer to estimate the total disturbance $\Delta = -\frac{1}{\alpha_1}(h + c_p F)$ and the state. Afterward, the hysteresis state h is estimated with a second observer. Finally, the estimated force $\hat{F}$ is derived using $\hat{\Delta}$ and $\hat{h}$.

3.1 Observer for $\Delta(t)$ and for position $y(t)$

The first differential equation of system Σ in (1) is rewritten as follows:

$$\dot{y} = -ay + bu + \Delta(t) \tag{3}$$

where $a = \frac{1}{\alpha_1}$, $b = \frac{d_p}{\alpha_1}$, and $\Delta(t) = -\frac{1}{\alpha_1}(h + c_p F)$; therefore,

$$\dot{\Delta}(t) = -\frac{1}{\alpha_1}\frac{d}{dt}(h + c_p F) = f(t). \tag{4}$$

Note that the hysteresis h and the force F are not directly measurable, making $\Delta(t)$ and its time derivative $\dot{\Delta}(t)$ unknown. In this work, $\Delta(t)$ is estimated,

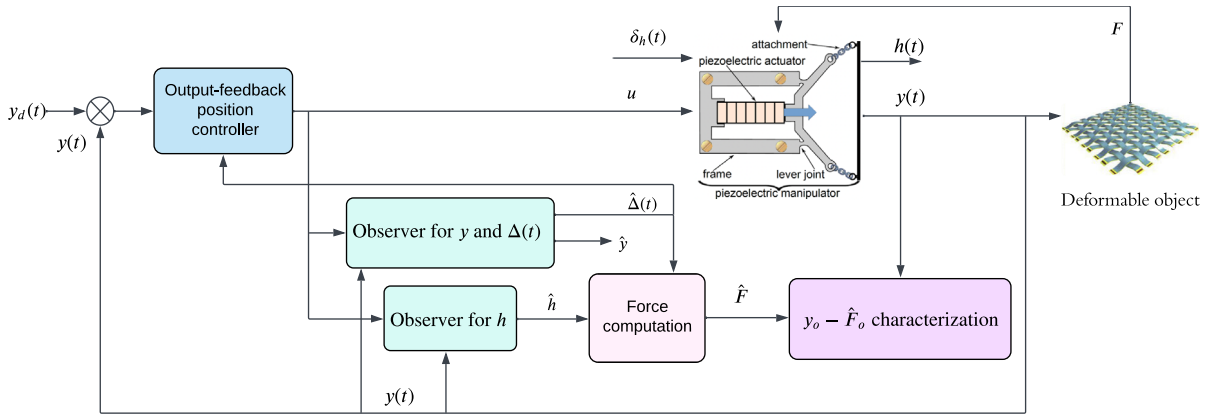

Fig. 2 General scheme illustrating the interaction between the deformable object, the output-feedback position controller, and the force computation module

which requires certain information about its behavior. Both terms $\frac{d}{dt}(h)$ and $\frac{d}{dt}(F)$ in (4) are bounded due to physical constraints:

- *Hysteresis* (h): The dynamics of hysteresis are limited by the material properties, such as elasticity and internal friction, ensuring that $\frac{d}{dt}(h)$ does not grow indefinitely.
- *Force* (F): The applied force F is bounded by the actuator's capabilities and external conditions, making $\frac{d}{dt}(F)$ inherently limited.

Consequently, $\dot{\Delta}(t)$ is bounded by a positive constant ϱ, which encapsulates the maximum rates of change for h and F. This justifies the inequality:

$$|\dot{\Delta}(t)| \leq \varrho. \tag{5}$$

The parameter ϱ is designed to be adaptable, allowing it to capture the observed dynamics in practical systems effectively. This adaptability ensures that inequality (5) remains valid under realistic conditions without imposing overly restrictive assumptions. Moreover, inequality (5) establishes a **practical bound**[1] [40–43] on $|\dot{\Delta}(t)|$, enhancing its utility in both theoretical and practical contexts.

With this foundation laid, the first main result is presented below.

Theorem 1 *Consider inequality (5). The system,*

$$\begin{aligned} \dot{\hat{y}} &= -a\hat{y} + bu + \hat{\Delta}(t) - (k_1)(\hat{y} - y) \\ \dot{\hat{\Delta}} &= \mu \end{aligned} \tag{6}$$

where $k_1, k_2 \in \mathbb{R}_{>0}$, $a + k_1 > k_2$, *with correction term*

$$\mu = -(\hat{y} - y) + (k_2)(k_2 - a - k_1)(\hat{y} - y), \tag{7}$$

is a globally uniformly bounded (GUB) extended observer for system (3).

Proof The observer errors are defined as follows:

$$\varepsilon_1 = \hat{y} - y, \quad \varepsilon_2 = \hat{\Delta} - \Delta \tag{8}$$

whose dynamics using (4) and (6) is given by,

$$\begin{aligned} \dot{\varepsilon}_1 &= -(a + k_1)\varepsilon_1 + \varepsilon_2 \\ \dot{\varepsilon}_2 &= \mu(\varepsilon_1) - f(t). \end{aligned} \tag{9}$$

A Backstepping-like procedure is followed to demonstrate that the errors (8) converge to zero. First, consider the change of coordinates:

$$\bar{\varepsilon}_1 = \varepsilon_1, \qquad \bar{\varepsilon}_2 = \varepsilon_2 - g(\varepsilon_1), \tag{10}$$

where $g(\varepsilon_1)$ is a function to be designed later. The dynamics of (9) in the coordinates (10) is now:

$$\begin{aligned} \dot{\bar{\varepsilon}}_1 &= -(a + k_1)\bar{\varepsilon}_1 + \bar{\varepsilon}_2 + g(\bar{\varepsilon}_1) \\ \dot{\bar{\varepsilon}}_2 &= \mu(\bar{\varepsilon}_1) - f(t) - \frac{\partial g(\bar{\varepsilon}_1)}{\partial \bar{\varepsilon}_1} \frac{\mathrm{d}}{\mathrm{dt}} \bar{\varepsilon}_1. \end{aligned} \tag{11}$$

The focus is placed on the first equation of (11). The quadratic Lyapunov function $\mathcal{V}_1 = \frac{1}{2}\bar{\varepsilon}_1^2$ is proposed, whose time derivative along the trajectories of the first equation of (11) is given by:

$$\dot{\mathcal{V}}_1 = (\bar{\varepsilon}_1)\left(-(a + k_1)\bar{\varepsilon}_1 + \bar{\varepsilon}_2 + g(\bar{\varepsilon}_1)\right). \tag{12}$$

$g(\bar{\varepsilon}_1) = k_2\bar{\varepsilon}_1$ is chosen, and (12) is simplified to:

$$\dot{\mathcal{V}}_1 = (k_2 - [a + k_1])\bar{\varepsilon}_1^2 + \bar{\varepsilon}_1\bar{\varepsilon}_2. \tag{13}$$

[1] Practical bounds are designed to be flexible, robust, and conducive to simplifying design and stability analysis, while maintaining applicability to real-world scenarios.

Then, the second equation in (11) is addressed by proposing the Lyapunov function $\mathcal{V}_2 = \mathcal{V}_1 + \frac{1}{2}\bar{\varepsilon}_2^2$, whose time derivative along the trajectories of the second equation in (11) is given by:

$$\dot{\mathcal{V}}_2 = \dot{\mathcal{V}}_1 + \bar{\varepsilon}_2\left(\mu(\bar{\varepsilon}_1) - f(t) - \frac{\partial g(\bar{\varepsilon}_1)}{\partial \bar{\varepsilon}_1}\frac{\mathrm{d}}{\mathrm{dt}}\bar{\varepsilon}_1\right). \quad (14)$$

Once $g(\bar{\varepsilon}_1) = k_2\bar{\varepsilon}_1$ is chosen, it follows that:

$$\dot{g}(\bar{\varepsilon}_1) = \frac{\partial g(\bar{\varepsilon}_1)}{\partial \bar{\varepsilon}_1}\frac{\mathrm{d}}{\mathrm{dt}}\bar{\varepsilon}_1 = (k_2)(k_2 - a - k_1)\bar{\varepsilon}_1 + k_2\bar{\varepsilon}_2, \quad (15)$$

and then, (14) can be rewritten as:

$$\begin{aligned}\dot{\mathcal{V}}_2 = &\Big(k_2 - [a + k_1]\Big)\bar{\varepsilon}_1^2 + \bar{\varepsilon}_1\bar{\varepsilon}_2 \\ &+ \bar{\varepsilon}_2\Big(\mu(\bar{\varepsilon}_1) - f(t) - (k_2)(k_2 - a - k_1)\bar{\varepsilon}_1 - k_2\bar{\varepsilon}_2\Big),\end{aligned} \quad (16)$$

where $\mu(\bar{\varepsilon}_1)$ is chosen as in (7), and (16) is thus simplified to:

$$\begin{aligned}\dot{\mathcal{V}}_2 &= -([a + k_1] - k_2)\bar{\varepsilon}_1^2 - k_2\bar{\varepsilon}_2^2 - f(t)\bar{\varepsilon}_2 \\ &\leq -([a + k_1] - k_2)\bar{\varepsilon}_1^2 - k_2\bar{\varepsilon}_2^2 + \varrho|\bar{\varepsilon}_2|\end{aligned} \quad (17)$$

where we have claimed (5). Then,

$$\begin{aligned}&\dot{\mathcal{V}}_2 \leq -([a + k_1] - k_2)\bar{\varepsilon}_1^2 - k_2\bar{\varepsilon}_2^2 + \varrho|\bar{\varepsilon}_2|, \\ &\forall|\bar{\varepsilon}_2| > \frac{\varrho}{k_2}.\end{aligned} \quad (18)$$

If we define the vector $\bar{\varepsilon} = \begin{bmatrix}\bar{\varepsilon}_1 \\ \bar{\varepsilon}_2\end{bmatrix}$ and its square norm as $\|\bar{\varepsilon}\| = \sqrt{\bar{\varepsilon}_1^2 + \bar{\varepsilon}_2^2}$, it follows that $|\bar{\varepsilon}_2| \leq \|\bar{\varepsilon}\| = \sqrt{\bar{\varepsilon}_1^2 + \bar{\varepsilon}_2^2}$. Thus, we can express $\dot{\mathcal{V}}_2$ as follows:

$$\dot{\mathcal{V}}_2 \leq -\bar{\varepsilon}^\top Q\bar{\varepsilon} + \varrho\|\bar{\varepsilon}\|, \quad (19)$$

where

$$Q = \begin{bmatrix}(a + k_1) - k_2 & 0 \\ 0 & k_2\end{bmatrix} \quad (20)$$

is a positive definite matrix. Then,

$$\dot{\mathcal{V}}_2 \leq -\lambda_{\min}(Q)\|\bar{\varepsilon}\|^2, \quad \forall\|\bar{\varepsilon}\| \geq \frac{\varrho}{2k_2}. \quad (21)$$

This ensures that the system exhibits global ultimate boundedness (GUB) with a bound proportional to $\frac{\varrho}{2k_2}$ as long as $k_2 < a + k_1$. □

Remark 2 The size of the ultimate bounded region can be made arbitrarily small by appropriately tuning the gains k_1 and k_2, ensuring that the system's response remains within a desired performance threshold.

3.2 Observer for the hysteresis state h

System Σ is rewritten with notation as in (3) as follows:

$$\begin{aligned}\dot{y} &= -ay + bu - ah + \delta_y(t) \\ \dot{h} &= A_{bw}\dot{u} - B_{bw}|\dot{u}|h - \Gamma_{bw}\dot{u}|h| + \delta_h(t)\end{aligned} \quad (22)$$

where $\delta_y(t) = -\frac{c_p}{\alpha_1}F$ is considered an unknown term. The previous equations can be rewritten in vector form as follows,

$$\dot{z} = Az + \phi(z, \dot{u}, u) + \delta(t), \quad \zeta = Cz, \quad (23)$$

where $z = \big(y,\ h\big)^\mathsf{T}$, $A = \begin{pmatrix}0 & -a \\ 0 & 0\end{pmatrix}$, $\delta(t) = \big(\delta_y,\ \delta_h\big)^\mathsf{T}$, $C = \big(1,\ 0\big)$, and

$$\begin{aligned}&\phi(z, \dot{u}, u) \\ &= \big(-ay + bu,\ A_{bw}\dot{u} - B_{bw}|\dot{u}|h - \Gamma_{bw}\dot{u}|h|\big)^\mathsf{T}.\end{aligned} \quad (24)$$

Lemma 1 *System (23) is observable as long as* $\alpha_1 \neq 0$.

Proof Please see our previous work [30]. □

Assumption 4 $|u| \leq \sup\{|u(t)|\}_{t\geq 0} = \mu_1 \in \mathbb{R}_{\geq 0}$ and $|\dot{u}| \leq \sup\{|\dot{u}(t)|\}_{t\geq 0} = \mu_2 \in \mathbb{R}_{\geq 0}$.

Assumption 5 The vector $\delta(t)$ has a bound expressed by,

$$\|\delta(t)\| \leq \rho\|\epsilon\|, \text{ with } \rho > 0 \quad (25)$$

where $\epsilon = \hat{z} - z$ is the state error of observer (26) and system (23).

Theorem 2 *Consider that Assumptions 4 and 5 hold. Additionally, consider the constants* $\kappa > 1/2$ *and* $\theta > 2\left(L_\phi + \rho\right)\frac{\lambda_{max}\{S\}}{\lambda_{min}\{S\}}$, *where* L_ϕ *is a Lipschitz constant defined in the proof of this theorem. Then, the system,*

$$\begin{aligned}\dot{\hat{z}} &= A\hat{z} + \phi(\hat{z}, \dot{u}, u) - \kappa S^{-1}QC^\mathsf{T}\left(C\hat{z} - Cz\right) \\ \dot{S} &= -\theta S - A^\mathsf{T}S - SA + QC^\mathsf{T}C\end{aligned} \quad (26)$$

is an exponential observer for system (23), where $S(0) \succ 0$, *and* Q *is a positive definite diagonal matrix.*

Proof The error observer in Assumption 5 has dynamics:

$$\dot{\epsilon} = \left(A - \kappa S^{-1}QC^\mathsf{T}C\right)\epsilon + \phi(\hat{z}, \dot{u}, u) - \phi(z, \dot{u}, u) - \delta(t). \quad (27)$$

The candidate Lyapunov function $\mathcal{W} = \epsilon^\intercal S \epsilon$ is proposed, with its first-time derivative along the trajectories of (27) given by,

$$\begin{aligned}\dot{\mathcal{W}} &= 2\epsilon^\intercal S\dot{\epsilon} + \epsilon^\intercal \dot{S}\epsilon \\ &= 2\epsilon^\intercal S\Big[\Big(A - \kappa S^{-1} QC^\intercal C\Big)\epsilon + \phi(\hat{z}, \dot{u}, u) - \phi(z, \dot{u}, u) \\ &\quad - \delta(t)\Big] + \epsilon^\intercal\Big[-\theta S - A^\intercal S - SA + QC^\intercal C\Big]\epsilon \\ &= \epsilon^\intercal\Big(SA - A^\intercal S - \theta S - [2\kappa - 1]QC^\intercal C\Big)\epsilon \\ &\quad + 2\epsilon^\intercal S\Big(\phi(\hat{z}, \dot{u}, u) - \phi(z, \dot{u}, u) - \delta(t)\Big).\end{aligned} \tag{28}$$

Since $\epsilon^\intercal (SA - A^\intercal S)\,\epsilon = 0$, (28) is simplified to,

$$\begin{aligned}\dot{\mathcal{W}} &= -\theta\epsilon^\intercal S\epsilon - (2\kappa - 1)\,\epsilon^\intercal QC^\intercal C\epsilon \\ &\quad + 2\epsilon^\intercal S\Big(\phi(\hat{z}, \dot{u}, u) - \phi(z, \dot{u}, u) - \delta(t)\Big) \\ &\leq -\theta\epsilon^\intercal S\epsilon + 2\epsilon^\intercal S\Big(\phi(\hat{z}, \dot{u}, u) - \phi(z, \dot{u}, u) - \delta(t)\Big).\end{aligned} \tag{29}$$

Notice that $\phi(z, \dot{u}, u)$ is global Lipschitz with respect to z uniformly in $\dot{u}$ and u (see Lemma 2 below). Thus,

$$\begin{aligned}\dot{\mathcal{W}} &\leq -\theta\epsilon^\intercal S\epsilon + 2L_\phi\|S\epsilon\|\|\epsilon\| + 2\rho\|S\epsilon\|\|\epsilon\| \\ &\leq -\theta\epsilon^\intercal S\epsilon + 2\left(L_\phi + \rho\right)\|S\epsilon\|\|\epsilon\|,\end{aligned} \tag{30}$$

where L_ϕ is the Lipschitz constant for function $\phi(\cdot)$. After simple computations similar to [29], (30) is rewritten as,

$$\dot{\mathcal{W}} \leq -\left(\theta - 2\left(L_\phi + \rho\right)\frac{\lambda_{\max}\{S\}}{\lambda_{\min}\{S\}}\right)\mathcal{W}. \tag{31}$$

By choosing $\theta > 2\left(L_\phi + \rho\right)\frac{\lambda_{\max}\{S\}}{\lambda_{\min}\{S\}}$, and since $\mathcal{W}$ is radially unbounded, global exponential stability of the observer error ϵ is obtained, as expected. □

3.3 Derivation of the force

Remind that from the model (1), we denote the total disturbance as $\Delta(t) = -h - c_p F$. Since we now have an estimation of the disturbance Δ and an estimation of the hysteresis state h, the force F that resists the actuator's position can be deduced as follows:

$$\hat{F} = -\frac{1}{c_p}\left(\hat{\Delta} + \hat{h}\right). \tag{32}$$

It is reminded that the object reaction force F_o is given by $F_o = \frac{1}{k_m}\hat{F}$, where a lever mechanism gain of $k_m = 1$ is chosen.

4 Output feedback law

It is noted that the hysteresis equation of system Σ, as depicted in (1), cannot be readily manipulated through direct control input. Additionally, it is worth mentioning that the positioning subsystem, among other factors, relies on this hysteresis term. Therefore, it must be demonstrated that the solutions of the entire system Σ are bounded under bounded inputs. This critical insight is elucidated in the following lemma.

Lemma 2 *Assume that Assumption 4 holds, and consider that the force F and disturbance $\delta_h(t)$ are bounded as:*

$$\begin{aligned}|F| &\leq \sup\{|F(t)|\}_{t\geq 0} = c_1 \in \mathbb{R}_{\geq 0} \\ |\delta_h| &\leq \sup\{|\delta_h(t)|\}_{t\geq 0} = c_2 \in \mathbb{R}_{\geq 0}.\end{aligned} \tag{33}$$

Also assume that $a > 1$, and $B_{bw} > |\Gamma_{bw}| + \frac{a+1}{2\mu_2}$ hold. Then, all the solutions of system Σ in (1) are uniformly bounded.

Proof The proof consists of finding a Lyapunov function with time-derivative evaluated in the trajectories of system Σ such that it remains bounded for all possible system states.

The candidate Lyapunov function $V_0 = \frac{1}{2}y^2 + \frac{1}{2}h^2$ is proposed. Its first time derivative is computed along the system Σ trajectories expressed as in (22):

$$\begin{aligned}\dot{V}_0 &= y\left(-ay + bu - ah + \delta_y(t)\right) \\ &\quad + h\left(A_{bw}\dot{u} - B_{bw}\,|\dot{u}|\,h - \Gamma_{bw}\dot{u}\,|h| + \delta_h(t)\right) \\ &\leq -ay^2 - B_{bw}\mu_2 h^2 + \mu_1|b||y| - ayh + c_1|c_p a||y| \\ &\quad + \mu_2|A_{bw}||h| + \mu_2|\Gamma_{bw}|h^2 + c_2|h|\end{aligned} \tag{34}$$

where (33) and Assumption 4 have been used. Consider the Young inequality applied in the cross term:

$$-ayh = -(\sqrt{a}y)(\sqrt{a}h) \leq \frac{1}{2}ay^2 + \frac{1}{2}ah^2. \tag{35}$$

Then, the following is obtained:

$$\begin{aligned}\dot{V}_0 &\leq -\left(a - \frac{1}{2}a\right)y^2 - \left(B_{bw}\mu_2 - \mu_2|\Gamma_{bw}| - \frac{1}{2}a\right)h^2 \\ &\quad + \left(\mu_1|b| + c_1|c_p a|\right)|y| + \left(\mu_2|A_{bw}| + c_2\right)|h|.\end{aligned} \tag{36}$$

The Young inequality is applied to the last two terms of (36):

$$\begin{aligned}\left(\mu_1|b| + c_1|c_p a|\right)|y| &\leq \frac{1}{2}\left(\mu_1|b| + c_1|c_p a|\right)^2 + \frac{1}{2}y^2\\ \left(\mu_2|A_{bw}| + c_2\right)|h| &\leq \frac{1}{2}\left(\mu_2|A_{bw}| + c_2\right)^2 + \frac{1}{2}h^2.\end{aligned} \tag{37}$$

Finally, (36) is expressed as,

$$\begin{aligned}\dot{V}_0 \leq -\frac{1}{2}(a-1)y^2 - \left(B_{bw}\mu_2 - \mu_2|\Gamma_{bw}| - \frac{1}{2}a - \frac{1}{2}\right)h^2\\ + \underbrace{\frac{1}{2}\left(\left(\mu_1|b| + c_1|c_p a|\right)^2 + \left(\mu_2|A_{bw}| + c_2\right)^2\right)}_{r}.\end{aligned} \tag{38}$$

Since a is positive by definition of system Σ, it is possible to choose $a > 1$, and $B_{bw} > |\Gamma_{bw}| + \frac{a+1}{2\mu_2}$. In that case, $\dot{V}_0 \leq -\psi V_0 + L$ where $L > r$ and $\psi \in \mathbb{R}_{>0}$ can be appropriate chosen to achieve the above inequality. Following a similar procedure as in [44], it is easily demonstrated that the system states are bounded under the Lemma conditions. □

To solve Problem 1, the result of Lemma 2 is considered. In this case, since the hysteresis is demonstrated to be bounded, the focus can be placed only on the first equation of system Σ, i.e., (3). Then, the observer presented in Theorem 1 is used. The result is provided below.

Theorem 3 *The system (3) and the observer (6) are consider under the conditions stated in Theorem 1 and its corresponding proof. Then, the output feedback control law,*

$$u = \frac{1}{b}\left(ay - \hat{\Delta}(t) + \dot{y}_d - ke\right) \tag{39}$$

where $k > 0$, ensures that the observer errors (8) and the tracking error

$$e = y - y_d, \tag{40}$$

exhibit global ultimate boundedness (GUB) as long as $\lambda_{\min}(Q) > \frac{\varphi_1^2\left(l_{G_1}+l_F\right)^2\sigma}{4\varphi_2}$ where Q is defined in (20) and the terms on the right-hand side of the previous inequality are positive and are explicitly defined in the proof of this theorem. Moreover, the ultimate bound on the errors can be made arbitrarily small by appropriately choosing the control gains.

Proof The tracking error dynamics is given by,

$$\dot{e} = -a(e + y_d) + bu + \Delta(t) - \dot{y}_d. \tag{41}$$

The candidate Lyapunov function $V = \frac{1}{2}e^2$ is proposed, with its time derivative along the trajectories of (41) given by:

$$\dot{V} = e\left(-a(e + y_d) + bu + \Delta(t) - \dot{y}_d\right). \tag{42}$$

For a moment, let it be assumed that $\Delta(t)$ is available for feedback in the control law (39), i.e., $u = \frac{1}{b}\left(ay - \Delta(t) + \dot{y}_d - k[y - y_d]\right)$. Then, (42) is simplified to $\dot{V} = -ke^2$. This show us that substituting an estimate of $\Delta(t)$ that converges to it in the control law, will result in a closed-loop stable error dynamic system.

Based on the previous analysis, the proof is continued for the closed-loop system with the output feedback control (39). First, the observer error dynamics (11) and the tracking error dynamics (41) are recalled and rewritten below in closed-loop form with the control (39) in coordinates (10), (40):

$$\begin{aligned}\dot{e} &= -ke - (\bar{\varepsilon}_2 + g(\bar{\varepsilon}_1)) =: F(e, \bar{\varepsilon})\\ \dot{\bar{\varepsilon}}_1 &= -(a + k_1)\bar{\varepsilon}_1 + \bar{\varepsilon}_2 + g(\bar{\varepsilon}_1) =: G_1(\bar{\varepsilon})\\ \dot{\bar{\varepsilon}}_2 &= \mu(\bar{\varepsilon}_1) - f(t) - \frac{\partial g(\bar{\varepsilon}_1)}{\partial \bar{\varepsilon}_1}\frac{\mathrm{d}}{\mathrm{dt}}\bar{\varepsilon}_1 =: G_2(\bar{\varepsilon}, t).\end{aligned} \tag{43}$$

The above equations can be rewritten using $\bar{\varepsilon} = \left(\bar{\varepsilon}_1\ \bar{\varepsilon}_2\right)^\mathsf{T}$ and the change of coordinates $\xi = e + \bar{\varepsilon}_1 = (y - y_d) + (\hat{y} - y) = \hat{y} - y_d$ as follows:

$$\begin{aligned}\dot{\xi} &= F(\xi - \bar{\varepsilon}_1, \bar{\varepsilon}) + G_1(\bar{\varepsilon})\\ \dot{\bar{\varepsilon}} &= G(\bar{\varepsilon}, t).\end{aligned} \tag{44}$$

With the above system, it needs to be proven that $(\xi, \bar{\varepsilon}) \in \mathbb{R}^3$ is globally ultimately bounded. To achieve this, the Lyapunov functions V and $\mathcal{V}_2$ are reconsidered to design the candidate Lyapunov function $\mathcal{L} = \sigma V(\xi) + \mathcal{V}_2(\bar{\varepsilon})$ with $\sigma > 0$. The time-derivative of $\mathcal{L}$ is computed along the trajectories of system (44) as follows:

$$\dot{\mathcal{L}} = \sigma\frac{\partial V(\xi)}{\partial \xi}\left(F(\xi - \bar{\varepsilon}_1, \bar{\varepsilon}) + G_1(\bar{\varepsilon})\right) + \dot{\mathcal{V}}_2(\bar{\varepsilon}). \tag{45}$$

To (45), $\sigma\frac{\partial V(\xi)}{\partial \xi}F(\xi, \bar{\varepsilon})$ is added and subtracted, resulting in:

$$\begin{aligned}\dot{\mathcal{L}} &= \sigma\frac{\partial V(\xi)}{\partial \xi}F(\xi, \bar{\varepsilon}) + \dot{\mathcal{V}}_2(\bar{\varepsilon})\\ &\quad + \sigma\frac{\partial V(\xi)}{\partial \xi}\left(G_1(\bar{\varepsilon}) + F(\xi - \bar{\varepsilon}_1, \bar{\varepsilon}) - F(\xi, \bar{\varepsilon})\right)\end{aligned} \tag{46}$$

Since $F(\cdot)$ and $G_1(\cdot)$ are Lipschitz continuous, with respective Lipschitz constants l_F and l_{G_1}, it follows that:

$$\dot{\mathcal{L}} \leq \sigma \frac{\partial V(\xi)}{\partial \xi} F(\xi, \bar{\varepsilon}) + \dot{\mathcal{V}}_2(\bar{\varepsilon}) + \sigma \left(l_{G_1} + l_F\right) \left\| \frac{\partial V(\xi)}{\partial \xi} \right\| \|\bar{\varepsilon}\|. \tag{47}$$

Also, thanks to Krasovsky [45], it follows that,

$$\dot{\mathcal{L}} \leq -\sigma\varphi_2 \|\xi\|^2 - \lambda_{\min}(Q)\|\bar{\varepsilon}\|^2 + \sigma\varphi_1 \left(l_{G_1} + l_F\right) \|\xi\| \|\bar{\varepsilon}\|, \quad \forall \|\bar{\varepsilon}\| \geq \frac{\varrho}{2k_2}. \tag{48}$$

The constants $\varphi_1, \varphi_2 > 0$, represent the Krasovsky bounds for the Lyapunov function derivative. By choosing $\lambda_{\min}(Q) > \frac{\varphi_1^2 (l_{G_1}+l_F)^2 \sigma}{4\varphi_2}$, it follows that $\dot{\mathcal{L}} < 0$, $\forall (\xi, \bar{\varepsilon}) \neq (0, 0)$ outside a bounded region, ensuring $(\xi, \bar{\varepsilon})$ is globally ultimately bounded. The size of the region can be reduced with appropriate tuning of the gains, especially k_2. □

Remark 3 Notice that the control law developed in Sect. 4 and the related observer in Sect. 3 are not at all designed with the deformable object model in (2). Therefore, the control law and the observer are not tuned with any object model and, consequently, are independent of that. Instead, the estimated force from the observer (designed without using the object model) and the actuator displacement permit the plotting (deformation, stress)-characteristics of the object without knowing à priori the latter's model. Also notice that the object model in (51), which is a case study related to the general object model in (2), is purely used to validate the proposed approach. A primary objective and significant contribution of the paper lies in our ability to design a control law and observer without relying on the object model for estimating its characteristics.

5 Simulation results

Two simulations are proposed. The first is to validate the control technique and the observers applied to the actuator model in (1) only, the force F inside it being considered an external disturbance. In the second simulation, the force F inside the actuator model of (1) is connected with the force model of (2), the target is to check a known object's (force, deformation)-characteristics. If the latter characteristics are consistent, then the control technique and the force observer applied to object characterization are effective.

The simulations were conducted using MATLAB Simulink with the ODE5 (Dormand-Price) solver, employing a fixed-step size of 0.0001 s, a start time of 0 s, and a stop time of 20 s. All simulation files are freely available for download at the following repository: https://github.com/gfloresc/ElasticManip.git

5.1 Feedback control simulation

Initially, the observers and feedback control from Sects. 3 and 4 are implemented on the actuator model defined by (1). The force F within the model, treated as an external disturbance in this initial simulation, is generated using a signal generator. The primary goal is to validate the effectiveness of the control technique along with the disturbance and observers.

The system parameters are taken from [30]. The values are $\alpha_1 = 0.001$, $d_p = 10$, $c_p = 0.002$, $A_{bw} = 0.4297$, $B_{bw} = 0.03438$, and $\Gamma_{bw} = -0.002865$. The goal is tracking the signal $y_d = 40 \sin(\frac{2\pi}{10} t)$. The parameters for the observer responsible to estimating $\Delta(t)$ are $k_1 = 700$, and $k_2 = 500$. The parameters for the hysteresis are given by: $\kappa = 200$, $\theta = 2000$, $Q = \begin{pmatrix} 6000 & 0 \\ 0 & 8000 \end{pmatrix}$, and $S(0) = \begin{pmatrix} 4 & 0.1 \\ 1 & 5 \end{pmatrix}$. The control parameter is $k = 1800$.

The results appear in Figs. 3, 4, and 5 where it is clear the effectiveness of the proposed observers and control as the latter show convergence.

5.2 Simulation with noise affecting the system

The proposed approach is presented in this section under the influence of exogenous noise to evaluate its performance. The closed-loop system (1)-(39) is modified as follows:

$$\begin{aligned} \alpha_1 \frac{dy}{dt} + y &= d_p u - h - c_p F + \eta_y(t), \\ \frac{dh}{dt} &= A_{bw} \frac{du}{dt} - B_{bw} \left| \frac{du}{dt} \right| h \\ &\quad - \Gamma_{bw} \frac{du}{dt} |h| + \delta_h(t) + \eta_h(t), \\ y &= Cz + \eta_m(t), \end{aligned} \tag{49}$$

where the noise terms $\eta_h(t)$, $\eta_y(t)$, and $\eta_m(t)$ are modeled as Gaussian noise with the following characteristics:

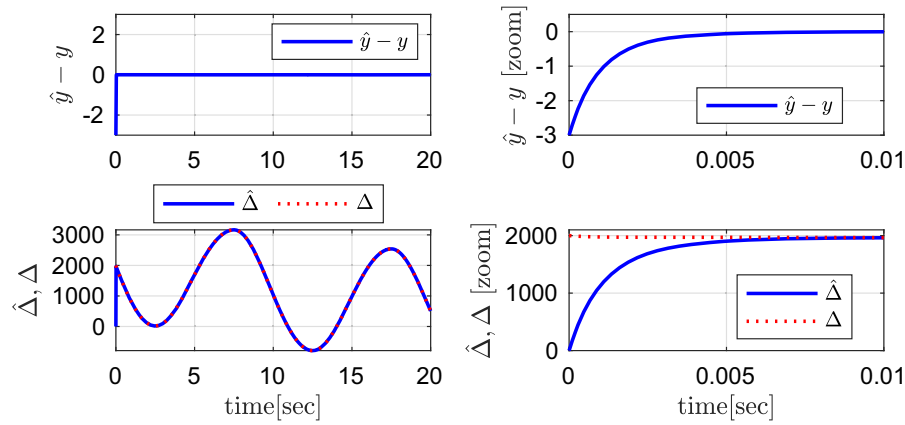

Fig. 3 The states convergence of the observer given in (6)

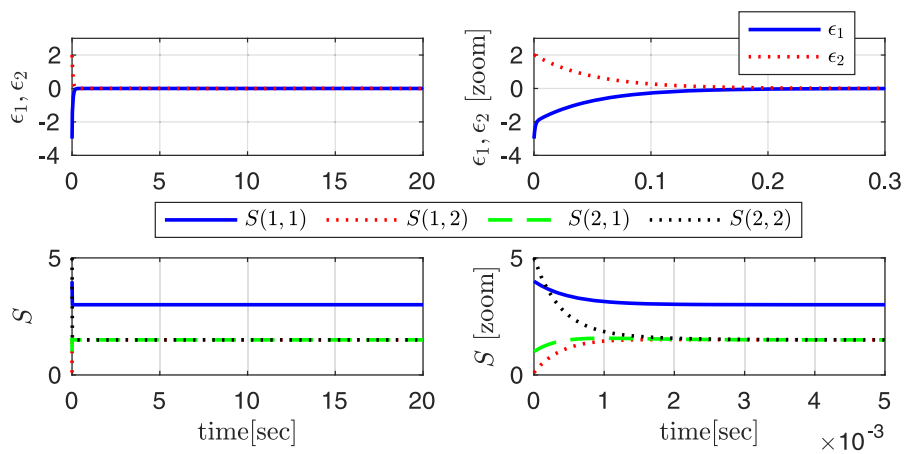

Fig. 4 The error state $\epsilon = (\epsilon_1 \ \epsilon_2)^\intercal$ convergence of (27), and the solution S of the Riccati-like equation given in (26)

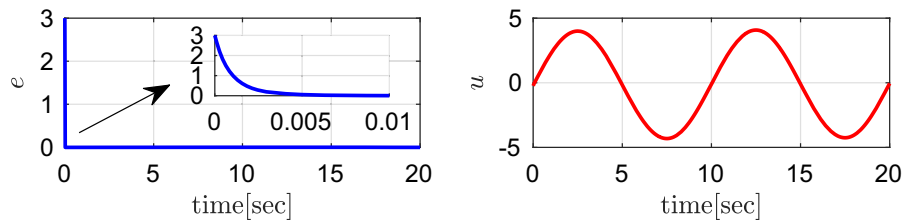

Fig. 5 The tracking error (40) and the control (39)

- $\eta_h(t) \sim \mathcal{N}(\mu, \sigma_h^2)$, where $\mu = 0$ and $\sigma_h^2 = 3$ ($\sigma_h = \sqrt{3}$),
- $\eta_y(t) \sim \mathcal{N}(\mu, \sigma_y^2)$, where $\mu = 0$ and $\sigma_y^2 = 5$ ($\sigma_y = \sqrt{5}$),
- $\eta_m(t) \sim \mathcal{N}(\mu, \sigma_m^2)$, where $\mu = 0$ and $\sigma_m^2 = 0.01$ ($\sigma_m = 0.1$).

All noise signals are sampled at $T_s = 0.001$ seconds, and a fixed random seed of 0 ensures the reproducibility of the noise sequences.

The control law incorporating noise is given by:

$$u = \frac{1}{b}\left(ay - \hat{\Delta}(t) + \dot{y}_d - ke\right) + \eta_u(t), \tag{50}$$

where the noise term $\eta_u(t)$ is modeled as Gaussian noise with $\eta_u(t) \sim \mathcal{N}(\mu, \sigma^2)$, where $\mu = 0$, $\sigma^2 = 0.01$ ($\sigma = 0.1$), and the signal is sampled at $T_s = 0.001$ seconds. A fixed random seed of 0 ensures reproducibility.

Gaussian noise with different variances has been applied to various components of the system, including the model dynamics, the control input, and the measurement output. It is worth noting that the most sensitive noise is that affecting the measurement, for obvious reasons. Nevertheless, the proposed control effectively mitigates the impact of the remaining noise terms

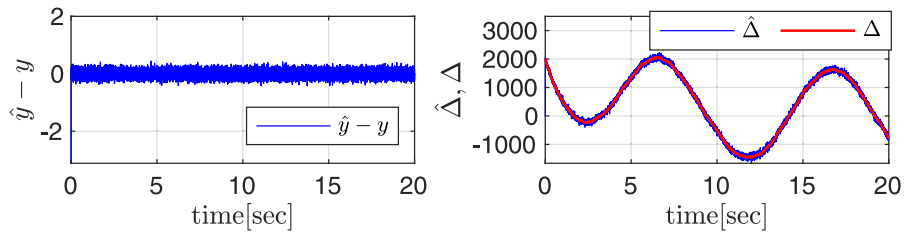

Fig. 6 Performance of the proposed observer under exogenous noise. The left plot shows the estimation error $\hat{y} - y$, demonstrating that the observer maintains accuracy despite the presence of measurement noise $\eta_m(t)$. The right plot compares the estimated disturbance $\hat{\Delta}$ (blue line) with the actual disturbance Δ (red line), showing that the observer effectively tracks the disturbance dynamics, even with added noise in the model and measurement

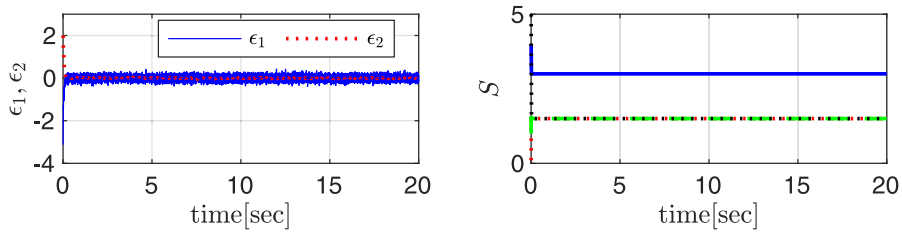

Fig. 7 Analysis of control and observer performance under noisy conditions. The left plot illustrates the observer error $\epsilon_1 = \hat{y} - y$ and $\epsilon_2 = \hat{h} - h$, confirming the observer's ability to maintain accurate tracking despite exogenous noise. The right plot shows the evolution of the entries of the matrix $\mathcal{S}$, used as a gain in the observer design, demonstrating stable and consistent behavior throughout the simulation

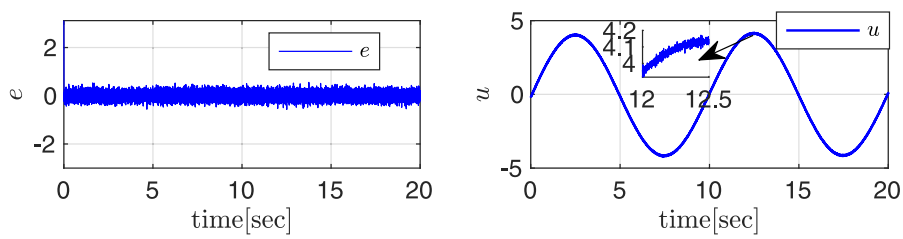

Fig. 8 Performance of the output feedback control under noise. The left plot shows the tracking error $e = y - y_d$, demonstrating the control's capability to maintain precise tracking despite the presence of noise. The right plot depicts the control input u, highlighting adaptability to noise-induced disturbances

within reasonable limits. The results are depicted in Figs. 6, 7, and 8.

5.3 Textile object characterization

The observers and the feedback control are now simulated when applied to the actuator model of (1). Contrary to the previous simulation, the force F inside the actuator model is due to the reaction of an object to be characterized. A miniaturized flax fiber fabric object inspired by [5] was chosen. It is a balanced plain weave composed of 100% desized-up flax fiber with the following properties: $458[g/m^2]$ of surface density, $380[/m]$ of warp density, $385[/m]$ of weft density. By using experimental data, a preliminary identification shows that the viscoelastic model of the object, (2), under tensile deformation can be represented as follows,

$$0.1\frac{dy}{dt} + y = 6\ln(F_o + 1) \tag{51}$$

Thus, the carried out simulation consists of the observers and the feedback control applied to the interconnection of the actuator model (1) with the object model (51). The estimated force $\hat{F}$, and thus $F_o = \hat{F}$, from the observer and the feedback-controlled output displacement y, and thus $y_o = y$, allows to plot the simulated (y_o, F_o)-map which is the characteristics of the object. It is compared with natural object behavior represented by (51). Figure 9 displays the results from a deformation reference $y_d = 14 \sin(2\pi f_r t) + 14$ of frequency $f_r = 1Hz$: continuous-line curve (—) represents the natural textile described by (51) and dots $(\cdots)$ represent the characteristics from the closed-loop and force observer. They show that both curves fit well; thus, the closed-loop and the force observer ensure enough precision for the characterization.

It is noted that instead of using the power law as in [36,37], the logarithmic function was proposed to approximate the experimental data: see the static terms in (51). Then, the first-order ODE extension is because viscoelastic behavior is observed in the deformation of many objects, including textiles [46].

Remark 4 The model (51) is identified from preliminary experimental characterization on a flax fiber fabric material. More precisely, the flax fiber material was the same as that used in [4], and various experimental works, including tensile and shear tests, were carried out during the preparation of that paper [4]. A tensile experiment on a miniaturized sample, which was not presented in [4] as that reference only included large samples, was conducted and identified to result in the model of (51).

5.4 Comments about simulations

The first simulation was carried out with a non-zero force generated by a signal generator. The first simulation aims to validate the feedback control and the disturbance Δ observer for any non-zero force considered as a disturbance. Note that the feedback control and the observer were only designed with the actuator model without considering any object model. On the other hand, the second simulation was carried out with force due to the reaction of an object to be characterized and thus to provide the characteristics of this object. To this aim, a viscoelastic model of the object is first given based on previous experimental data. Then, the simulation applies the proposed control law and observers (designed without an object model) to the actuator model interconnected with the object model through the interaction force. Afterward, the estimated force from the observer is plotted versus the controlled actuator displacement. This force-displacement plot is compared with the force-displacement plot purely from the object model (supposed to represent the experimental data). The comparison in Fig. 9 shows consistency, demonstrating the effectiveness of the control law and observers (once again designed without an object model) to characterize an object's behavior.

5.5 Comparison

The work of this paper is now compared with the previous work in [30]. Both this paper and the paper in [30] are designing a control law for a piezoelectric manipulator exhibiting strong hysteresis nonlinearity modeled with the Bouc-Wen approach. However, in this paper, the interaction force with the external environment is estimated and accounted for in the control law design, while in [30], it is not estimated nor accounted for. The tracking errors for both cases are depicted in Fig. 10. The same system parameters described were used to obtain the simulation results for both scenarios. The tracking error e corresponds to our proposed closed-loop system, while the tracking error e_0 corresponds to the closed-loop system response when using the controller in [30]. The considerable effect due to the applied force in e_0 can be observed (using [30]), demonstrating the superiority of the work presented in this paper.

The paper in [44] also treats the control law design for piezoelectric manipulators exhibiting strong hysteresis nonlinearity. It uses a Dahl as a hysteresis model. The feedback control law accounted for and rejected the force considered a disturbance. However, the paper [44] does not estimate the force and thus cannot be used for a characterization application contrary to the work in this paper.

6 Conclusions

An output feedback control technique was proposed for a piezoelectric manipulator during textile characterization. While the actuator was strongly nonlinear,

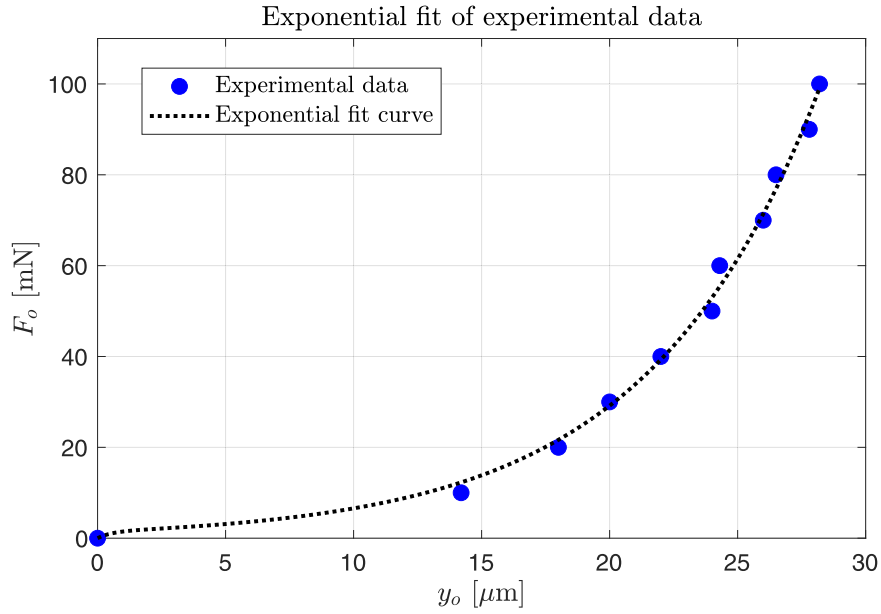

Fig. 9 (y_o, F_o)-map of a miniaturized flax fiber fabric. The dotted black line is obtained by plotting (y, F)-map from (51). This equation is the viscoelastic model identified from experimental data on a real flax fiber fabric. The blue dots-plot $(\cdots)$ is obtained by plotting (y, F) from the actuator model in the system model interconnected with the object model in (51) through F and controlled by the approach in Sect. 3 (observer) and Sect. 4 (feedback control). Therefore, the two graphs aim to compare if the feedback control with the observer (dots-plot) provides the same object-characteristic results as the real object characteristics (continuous-line plot). Note that $y_o = y$ and $F_o = F$ in both plotting

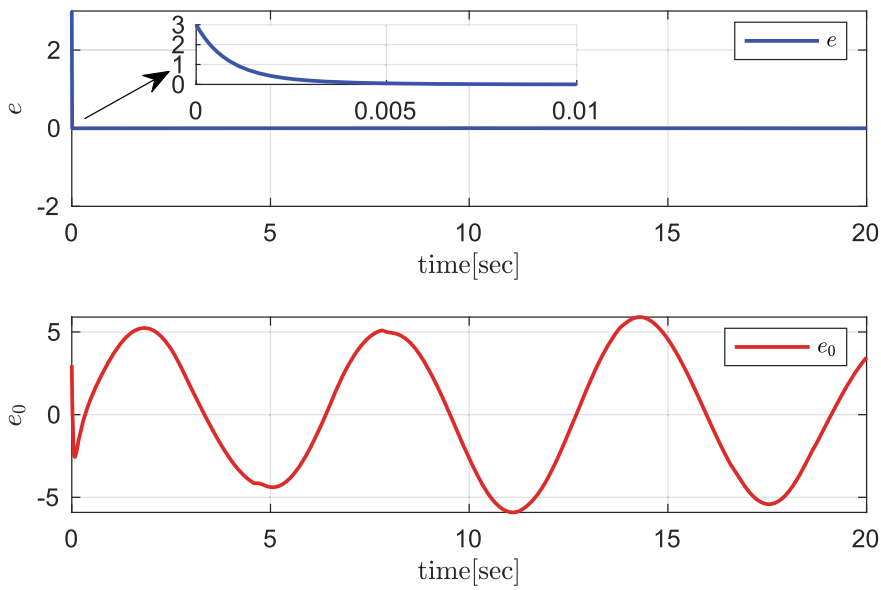

Fig. 10 The effect of the force in the position tracking error e_0 is considerable even with a small force. A force of $F = 3\sin(0.5t)$ was applied in this case

the controller design did not require knowledge of the object. To reach the target, the controller was designed with a classical Bouc-Wen that modeled the actuator's hysteresis nonlinearity and observers that estimated the actuator's states and the interaction force with the object. Various simulations were carried out, which show the effectiveness of the approach. From perspectives, an experimental benchmark will be mounted, and extensive experimental tests will be carried out for at least two materials of textile objects.

Supplementary information

All simulation files are freely available for download at the following repository: https://github.com/gfloresc/ElasticManip.git.

Author contributions Gerardo Flores: *Conceptualization:* Developed the main idea and designed the study. *Methodology:* Created the methods and procedures used in the research. *Data Analysis:* Processed and analyzed the results. *Writing - Original Draft:* Drafted the initial version of the manuscript. *Supervision:* Provided overall supervision and academic guidance for the project. Micky Rakotondrabe: *Conceptualization:* Developed the main idea and designed the study. *Investigation:* Conducted experiments and collected data. *Validation:* Verified the results and ensured data accuracy. *Writing - Review & Editing:* Critically reviewed and significantly contributed to improving the manuscript. *Resources:* Managed materials and tools necessary for the research.

Funding This work was partially supported by the CPER ECOSYSPRO project of UTTOP.

Data Availability Statement The datasets generated and/or analyzed during the current study are not publicly available but they are available from the corresponding author upon reasonable request.

Declarations

Conflict of interest The authors declare that they have no Conflict of interest.

Ethics approval and consent to participate Not applicable.

Consent for publication All authors have reviewed and approved the final version of the manuscript for submission and publication in the journal.

Materials availability Not applicable.

Code availability Not applicable.

References

1. Flores, G., Rakotondrabe, M.: Output feedback control of a piezoelectric robotic manipulator during the characterization of object exhibiting nonlinear viscoelastic deformation. In: American Control Conference (2024)
2. Mann, M.: Textile Design: Products and Processes, p. 268. CRC Press, United States (2020)
3. Dolez, P., Vermeersch, O., Izquierdo, V.: Advanced Characterization and Testing of Textiles. Woodhead Publishing, Cambridge, UK (2018)
4. Buet-Gautier, K., Boisse, P.: Experimental analysis and modeling of biaxial mechanical behavior of woven composite reinforcements. Exp. Mech. **41**, 260–269 (2001). https://doi.org/10.1007/BF02323143
5. Langat, K.R., Luycker, E.D., Noureddine, F., Rakotondrabe, M.: Robotic-assisted measurement of fabrics for the characterization of the shear tension coupling. Key Eng. Mater. **926**, 1303–1316 (2022). https://doi.org/10.4028/p-f0d0u9
6. Chen, X., Song, Y., Su, Z., Chen, H., Cheng, X., Zhang, J., Han, M., Zhang, H.: Flexible fiber-based hybrid nanogenerator for biomechanical energy harvesting and physiological monitoring. Nano Energy **38**, 43–50 (2017). https://doi.org/10.1016/j.nanoen.2017.05.047
7. Rakotondrabe, M.: Smart Materials-Based Actuators at the Micro/Nano-Scale. Springer, New York, NY (2020)
8. Song, G., Zhao, J., Zhou, X., De Abreu-Garcia, J.A.: Tracking control of a piezoceramic actuator with hysteresis compensation using inverse Preisach model. IEEE/ASME Trans. Mech. **10**(2), 198–209 (2005). https://doi.org/10.1109/TMECH.2005.844708
9. Oubellil, R., Ryba, Voda, A., Rakotondrabe, M.: Experimental model inverse-based hysteresis compensation on a piezoelectric actuator. In: 2015 19th International Conference on System Theory, Control and Computing (ICSTCC), pp. 186–191 (2015). https://doi.org/10.1109/ICSTCC.2015.7321291
10. Kuhnen, K., Janocha, H.: Inverse feedforwrad controller for complex hysteretic nonlinearities in smart-materials systems. Control Intell. Syst. **29**(3), 74–83 (2001)
11. Rakotondrabe, M.: Multivariable classical Prandtl-Ishlinskii hysteresis modeling and compensation and sensorless control of a nonlinear 2-DOF piezoactuator. Nonlinear Dynamics **89**, 481–499 (2017). https://doi.org/10.1007/s11071-017-3466-5
12. Al Janaideh, M., Krejcí, P.: Inverse rate-dependent Prandtl-Ishlinskii model for feedforward compensation of hysteresis in a piezomicropositioning actuator. IEEE/ASME Trans. Mech. **18**(5), 1498–1507 (2013). https://doi.org/10.1109/TMECH.2012.2205265
13. Rakotondrabe, M.: Bouc-Wen modeling and inverse multiplicative structure to compensate hysteresis nonlinearity in piezoelectric actuators. IEEE Trans. Autom. Sci. Eng. **8**(2), 428–431 (2011). https://doi.org/10.1109/TASE.2010.2081979
14. Habineza, D., Rakotondrabe, M., Gorrec, Y.L.: Multivariable generalized Bouc-Wen modeling, identification and feedforward control and its application to multi-DoF piezoelectric actuators. IFAC Proceed. Vol. **47**(3), 10952–10958

(2014). https://doi.org/10.3182/20140824-6-ZA-1003.01190
15. Croft, D., Shedd, G., Devasia, S.: Creep, hysteresis, and vibration compensation for piezoactuators: atomic force microscopy application. Am. Control Conf. **3**, 2123–21283 (2000). https://doi.org/10.1109/ACC.2000.879576
16. Rakotondrabe, M., Clevy, C., Lutz, P.: Complete open loop control of hysteretic, creeped, and oscillating piezoelectric cantilevers. IEEE Trans. Autom. Sci. Eng. **7**(3), 440–450 (2010). https://doi.org/10.1109/TASE.2009.2028617
17. Habineza, D., Zouari, M., Le Gorrec, Y., Rakotondrabe, M.: Multivariable compensation of hysteresis, creep, badly damped vibration, and cross couplings in multi-axes piezoelectric actuators. IEEE Trans. Autom. Sci. Eng. **15**(4), 1639–1653 (2018). https://doi.org/10.1109/TASE.2017.2772221
18. Devasia, S., Eleftheriou, E., Moheimani, S.O.R.: A survey of control issues in nanopositioning. IEEE Trans. Control Syst. Technol. **15**(5), 802–823 (2007). https://doi.org/10.1109/TCST.2007.903345
19. Cao, Y., Chen, X.B.: A survey of modeling and control issues for piezo-electric actuators. J. Dynamic Syst. Measurement Control **137**(1), 014001 (2014). https://doi.org/10.1115/1.4028055
20. Al Janaideh, M., Rakotondrabe, M.: Precision motion control of a piezoelectric cantilever positioning system with rate-dependent hysteresis nonlinearties. Nonlinear Dynamics **104**, 3385–3405 (2021). https://doi.org/10.1007/s11071-021-06460-w
21. Shan, Y., Leang, K.K.: Accounting for hysteresis in repetitive control design: Nanopositioning example. Automatica **48**(8), 1751–1758 (2012). https://doi.org/10.1016/j.automatica.2012.05.055
22. Qiao, Z., Gan, M., Wang, C.: Sliding mode control using linear extended state observer(LESO) and hysteresis compensator based on Bouc-Wen model in sinusoidal position control of a piezoelectric actuator. In: Proceedings of the 33rd Chinese Control Conference, pp. 3840–3845 (2014). https://doi.org/10.1109/ChiCC.2014.6895579
23. Zhang, Y., Yan, P., Zhang, Z.: Frequency-shaped sliding mode control of piezoelectric nano-stages with hysteresis estimation. ISA Trans. **107**, 340–349 (2020). https://doi.org/10.1016/j.isatra.2020.08.002
24. Chen, X., Hisayama, T.: Adaptive sliding-mode position control for piezo-actuated stage. IEEE Trans. Ind. Electron. **55**(11), 3927–3934 (2008). https://doi.org/10.1109/TIE.2008.926768
25. Li, Y., Xu, Q.: Adaptive sliding mode control with perturbation estimation and PID sliding surface for motion tracking of a piezo-driven micromanipulator. IEEE Trans. Control Syst. Technol. **18**(4), 798–810 (2010). https://doi.org/10.1109/TCST.2009.2028878
26. Ramli, M.H.M., Minh, T.V., Chen, X.: Pseudoextended Bouc-Wen model and adaptive control design with applications to smart actuators. IEEE Trans. Control Syst. Technol. **27**(5), 2100–2109 (2019). https://doi.org/10.1109/TCST.2018.2849735
27. Escareno, J.-A., Rakotondrabe, M., Habineza, D.: Backstepping-based robust-adaptive control of a nonlinear 2-DOF piezoactuator. Control Eng. Practice **41**, 57–71 (2015). https://doi.org/10.1016/j.conengprac.2015.04.007
28. Escareno, J., Abadie, J., Piat, E., Rakotondrabe, M.: Robust micro-positionnig control of a 2DOF piezocantilever based on an extended-state LKF. IFAC Mech. **58**, 82–92 (2019). https://doi.org/10.1016/j.mechatronics.2019.02.001
29. Flores, G., Rakotondrabe, M.: Classical Bouc-Wen hysteresis modeling and force control of a piezoelectric robotic hand manipulating a deformable object. IEEE Control Syst. Lett. **7**, 2413–2418 (2023). https://doi.org/10.1109/LCSYS.2023.3287142
30. Flores, G., Rakotondrabe, M.: Robust nonlinear control for a piezoelectric actuator in a robotic hand using only position measurements. IEEE Control Syst. Lett. **6**, 872–877 (2022). https://doi.org/10.1109/LCSYS.2021.3087102
31. Mabrok, M.A., Kallapur, A.G., Petersen, I.R., Lanzon, A.: Generalizing negative imaginary systems theory to include free body dynamics: Control of highly resonant structures with free body motion. IEEE Trans. Autom. Control **59**, 2692–2707 (2014). https://doi.org/10.1109/TAC.2014.2325692
32. Ling, J., Rakotondrabe, M., Feng, Z., Ming, M., Xiao, X.: A robust resonant controller for high-speed scanning of nanopositioners: Design and implementation. IEEE Trans. Control Syst. Technol. **28**(3), 1116–1123 (2020). https://doi.org/10.1109/TCST.2019.2899566
33. Flores, G., Aldana, N., Rakotondrabe, M.: Model predictive control based on the generalized Bouc-Wen model for piezoelectric actuators in robotic hand with only position measurements. IEEE Control Syst. Lett. **6**, 2186–2191 (2022). https://doi.org/10.1109/LCSYS.2021.3136456
34. Marzougui, S., Abdessalem, S.B., Faouzi, S.: Viscoelastic behavior of textile artificial ligaments. J. Appl. Sci. (2009). https://doi.org/10.3923/jas.2009.2794.2800
35. Haji, O., Blond, E.H., Hivet, G.,), J.B., Boisse, P., Durville, D., Roscoat, n. S.R.: Modèles de Comportement de Structures Textiles: Développement, Identification, Implémentation, (2018)
36. Toll, S., Månson, J.E.: Dynamics of a planar concentrated fiber suspension with non-hydrodynamic interaction. J. Rheology **38**(4), 985–997 (1994). https://doi.org/10.1122/1.550539
37. Wyk, C.M.: 20-note on the compressibility of wool. J. Textile Inst. Trans. **37**(12), 285–292 (1946). https://doi.org/10.1080/19447024608659279
38. Corre, S.L., Dumont, P., Orgéas, L., Favier, D.: Rheology of highly concentrated planar fiber suspensions. J. Rheology **49**(5), 1029–1058 (2005). https://doi.org/10.1122/1.1993594
39. Habineza, D., Rakotondrabe, M., Gorrec, Y.L.: Bouc-Wen modeling and feedforward control of multivariable hysteresis in piezoelectric systems: Application to a 3-DoF piezotube scanner. IEEE Trans. Control Syst. Technol. **23**(5), 1797–1806 (2015). https://doi.org/10.1109/TASE.2009.2028617
40. Khalil, H.K.: Nonlinear Systems. Prentice Hall, USA (2002)
41. Moreno, J.A., Osorio, M.: Strict Lyapunov functions for the super-twisting algorithm. IEEE Trans. Autom. Control **57**(4), 1035–1040 (2012). https://doi.org/10.1109/TAC.2012.2186179

42. Gonzalez, T., Moreno, J.A., Fridman, L.: Variable gain super-twisting sliding mode control. IEEE Trans. Autom. Control **57**(8), 2100–2105 (2012). https://doi.org/10.1109/TAC.2011.2179878
43. Rodríguez-Mata, A.E., Medrano-Hermosillo, J.A., López-Pérez, P.A., Gonzalez-Huitron, V.A., Castro-Linares, R., Cervantes-Rojas, J.S.: A novel fractional high-order sliding mode control for enhanced bioreactor performance. Fractal Fractional **8**(10), 607 (2024). https://doi.org/10.3390/fractalfract8100607
44. Flores, G., Rakotondrabe, M.: Dahl hysteresis modeling and position control of piezoelectric digital manipulator. IEEE Control Syst. Lett. **7**, 1021–1026 (2023). https://doi.org/10.1109/LCSYS.2022.3230472
45. Krasovsky, N.: Some Problems of Stability of Motion Theory, 1, ed Fizmatgiz, Moscow (1959)
46. Manich, A.M., Marino, P.N., Castellar, M.D., Saldivia, M., Sauri, R.M.: Viscoelastic modeling of natural and synthetic textile yarns. J. Appl. Polymer Sci. **76**(14), 2062–2067 (2000)